OPEN ACCESS
CellPress

Cell Reports
Article

Rictor/mTORC2 Loss in the *Myf5* Lineage Reprograms Brown Fat Metabolism and Protects Mice against Obesity and Metabolic Disease

Chien-Min Hung,[1] Camila Martinez Calejman,[1] Joan Sanchez-Gurmaches,[1] Huawei Li,[1] Clary B. Clish,[2] Simone Hettmer,[3,4,5,6,7] Amy J. Wagers,[3,4,5,6] and David A. Guertin[1,*]
[1]Program in Molecular Medicine, University of Massachusetts Medical School, Worcester, MA 01605, USA
[2]Broad Institute, Cambridge, MA 02142, USA
[3]Howard Hughes Medical Institute, USA
[4]Department of Stem Cell and Regenerative Biology, Harvard Stem Cell Institute, 7 Divinity Avenue, Cambridge, MA 01238, USA
[5]Joslin Diabetes Center, One Joslin Place, Boston, MA 02215, USA
[6]Department of Pediatric Oncology, Dana Farber Cancer Institute, Boston, MA 02155, USA
[7]Division of Pediatric Hematology/Oncology, Children's Hospital, Boston, MA 02155, USA
*Correspondence: david.guertin@umassmed.edu
http://dx.doi.org/10.1016/j.celrep.2014.06.007

SUMMARY

The in vivo functions of mechanistic target of rapamycin complex 2 (mTORC2) and the signaling mechanisms that control brown adipose tissue (BAT) fuel utilization and activity are not well understood. Here, by conditionally deleting *Rictor* in the *Myf5* lineage, we provide in vivo evidence that mTORC2 is dispensable for skeletal muscle development and regeneration but essential for BAT growth. Furthermore, deleting *Rictor* in *Myf5* precursors shifts BAT metabolism to a more oxidative and less lipogenic state and protects mice from obesity and metabolic disease at thermoneutrality. We additionally find that Rictor is required for brown adipocyte differentiation in vitro and that the mechanism specifically requires AKT1 hydrophobic motif phosphorylation but is independent of pan-AKT signaling and is rescued with BMP7. Our findings provide insights into the signaling circuitry that regulates brown adipocytes and could have important implications for developing therapies aimed at increasing energy expenditure as a means to combat human obesity.

INTRODUCTION

Adipose tissue is essential for many biological processes, and its dysfunction, for example in obesity, is associated with a growing spectrum of human diseases. Thus, understanding the developmental and metabolic regulation of adipose tissue has broad clinical implications. There are two main classifications of adipose tissue: white adipose tissue (WAT) and brown adipose tissue (BAT). WAT is the major energy storage site in the body and has critical endocrine functions (Gesta et al., 2007), whereas BAT dissipates energy as heat in a process called nonshivering thermogenesis (Cannon and Nedergaard, 2004). BAT is particularly important in small rodents and newborn humans to defend against cold exposure, and its functional relevance in adult humans was only recently appreciated (Harms and Seale, 2013; Nedergaard and Cannon, 2010; Tseng et al., 2010). Brown adipocytes are thermogenic because they express uncoupling protein 1 (UCP1), which embeds in the inner mitochondrial membrane and produces heat by uncoupling oxidative metabolism from ATP production. The energy expending properties of brown adipocytes coupled with the observation that human BAT amount inversely correlates with body fat mass is garnering interest in developing strategies to increase brown adipocyte number and/or activity to treat obesity (Harms and Seale, 2013; Nedergaard and Cannon, 2010; Tseng et al., 2010). However, the mechanisms, and in particular the signaling circuitry, by which BAT regulates its energy supply are poorly understood (Townsend and Tseng, 2014). With the obesity pandemic seemingly out of control, and with a desperate need for novel therapeutics, the importance of elucidating mechanisms controlling adipocyte growth and function cannot be overstated.

Studying the in vivo mechanisms of adipose tissue growth has been challenging because adipocyte origins are poorly understood, and consequently few tools are available for genetically targeting adipocyte precursors in vivo (e.g., by Cre-Lox). Lineage tracing studies indicate early mesenchymal precursor cells expressing *Myf5* give rise to myocytes, brown adipocytes, and a subset of white adipocytes (Sanchez-Gurmaches and Guertin, 2014; Sanchez-Gurmaches et al., 2012; Seale et al., 2008), and several recent studies have used the *Myf5-Cre* knockin allele (Tallquist et al., 2000) to study BAT development (Harms et al., 2014; Martinez-Lopez et al., 2013; Ohno et al., 2013; Sanchez-Gurmaches et al., 2012; Schulz et al., 2013). Thus, the multifate potential of *Myf5* precursors provides an opportunity to use genetics to distinguish between signaling mechanisms that are required in vivo for the growth of myocytes versus adipocytes.

The mechanistic target of rapamycin (mTOR) kinase is a master regulator of growth that functions in two distinct complexes

called mTORC1 (defined by the Raptor subunit) and mTORC2 (defined by the Rictor subunit) (Laplante and Sabatini, 2012). Although much is known about the inputs, outputs, and regulatory features of mTORC1, mTORC2 regulation and function remains more enigmatic. The best-described biochemical function of mTORC2 is to phosphorylate the hydrophobic motif (HM) of AKT (S473 in AKT1) and the related SGK (S422 in SGK1) kinases (García-Martínez and Alessi, 2008; Sarbassov et al., 2005). AKT has many effectors including GSK3β, FoxO1/3, and mTORC1 (through TSC2 and PRAS40), and most models indicate mTORC2 is an essential upstream regulator of pan-AKT activity (Laplante and Sabatini, 2012). However, the extent to which this is the case in vivo remains unclear because *Rictor*-deficient mouse embryo fibroblasts, which lack mTORC2, have seemingly normal GSK3β phosphorylation, mTORC1 activity, and only partially decreased FoxO1/3 phosphorylation (Guertin et al., 2006; Jacinto et al., 2006; Shiota et al., 2006).

Mice lacking *Rictor* die around embryonic day 10.5 (E10.5) (Guertin et al., 2006; Jacinto et al., 2006; Shiota et al., 2006); therefore, mTORC2 function in vivo is mostly being investigated using floxed *Rictor* alleles. In adipose tissue, two studies using *aP2-cre* to delete *Rictor* reported no effect on individual adipocyte size or overall adipose tissue mass (Cybulski et al., 2009; Kumar et al., 2010). One of the studies finds *aP2-cre;Rictor*$^{fl/fl}$ mice eventually develop mild glucose intolerance and ectopic lipid deposition, although a mechanism was not elucidated (Kumar et al., 2010). Notably however, the utility of *aP2-cre* to target adipocytes has recently been questioned (Lee et al., 2013; Mullican et al., 2013; Wang et al., 2013); therefore, the exact function of mTORC2 in adipose tissue remains unclear. Deleting *Rictor* in skeletal muscle with *Hsa-cre* or *Mck-cre* also has no effect on muscle fiber size or overall muscle mass and only minor effects on insulin-mediated glucose metabolism (Bentzinger et al., 2008; Kumar et al., 2008). These relatively mild phenotypes are somewhat surprising considering the importance of AKT signaling in metabolism; however, in both cases (adipose tissue and muscle), the Cre drivers used target mature cells, and thus the in vivo role of mTORC2 in adipose tissue and muscle precursors is unknown.

Here, we take advantage of the fact that *Myf5-Cre* expresses in precursors of muscle and brown adipocytes to investigate the role of Rictor (i.e., mTORC2) and for comparison Raptor (i.e., mTORC1) in muscle and BAT growth. We report that *Raptor* is essential in the *Myf5* lineage for myogenesis, establishing BAT precursors, and viability. In contrast, *Rictor* is dispensable for myogenesis and viability but essential for normal BAT growth. Moreover, Rictor-deficient BAT is more metabolically active, having elevated mitochondrial activity and decreased lipogenesis. Importantly, deleting *Rictor* in the *Myf5* lineage also augments diet-induced thermogenesis, which protects mice from an obesogenic diet at thermoneutrality. We additionally find that *Myf5*-lineage white adipocytes require Rictor for normal growth in vivo, suggesting a broader role for mTORC2 in adipose tissue development. Finally, we show that Rictor is also required in vitro for brown adipocyte differentiation, but not for pan-AKT activity, and that this differentiation defect is rescued with BMP7. Collectively, our results provide insight into the regulation of brown adipocytes and implicate Rictor/mTORC2 as a critical signaling node that balances oxidative and lipogenic metabolic states.

RESULTS

Rictor Is Dispensable in the *Myf5* Lineage during Embryogenesis

We investigated the role of mTORC1 versus mTORC2 in vivo in fat versus muscle development by generating *Myf5-Cre;Raptor*$^{fl/fl}$ (*Raptor*^{Myf5cKO}) and *Myf5-Cre;Rictor*$^{fl/fl}$ (*Rictor*^{Myf5cKO}) conditional knockout (KO) mice. The *Rictor*^{Myf5cKO} mice are born at the expected Mendelian ratio and show no obvious motor or behavioral defects (data not shown). In contrast, *Raptor*^{Myf5cKO} mice die perinatally. E16.5 *Raptor*^{Myf5cKO} embryos are smaller due to a muscle development defect that is not apparent in control or *Rictor*^{Myf5cKO} embryos (Figures S1A–S1D). Transverse sections through the head and neck of *Raptor*^{Myf5cKO} embryos reveal an underdeveloped tongue and the absence of the masseter, sternohyoid, hyglossus, supraspinatus, prevertebral, and trapezius muscles, the later deficiency resulting in hindneck body-wall fragility during specimen preparation (Figures S1A–S1D). Thus, *Raptor* is essential in the *Myf5* lineage for viability and muscle development, whereas *Rictor* is dispensable for both.

To confirm that *Rictor* is dispensable for myogenesis, we purified satellite cells (which express *Myf5*) from *Rictor*^{Myf5cKO} skeletal muscles, confirmed they are deleted for *Rictor* (Figure S1E), and show they differentiate ex vivo into myosin heavy chain-positive multinucleate myofibers (Figures S1F and S1G). Moreover, deleting *Raptor* in satellite cells in vivo with *Pax7*-CreER blocks skeletal muscle repair, whereas deleting *Rictor* by the same approach does not prevent muscle regeneration following acute injury (Figures S1H and S1I). Thus, Rictor is also dispensable for satellite cell differentiation ex vivo and for adult myogenesis induced by injury.

WATs develop postpartum in mice, but early brown adipocyte precursor cells (bAPCs) are detectable in E16.5 embryos by hematoxylin and eosin (H&E) staining. Qualitatively similar pools of cervical, interscapular, and subscapular bAPCs are detectable in control and *Rictor*^{Myf5cKO} E16.5 embryos (Figures S1A and S1D). In contrast, interscapular and subscapular bAPCs are absent in E16.5 *Raptor*^{Myf5cKO} embryos (Figures S1A and S1D). Notably, a diminished pool of cervical bAPCs is detectable in the *Raptor*^{Myf5cKO} embryos consistent with our lineage tracing data showing that only about half of the cervical brown adipocytes arise from *Myf5-Cre*-expressing precursors (Figure S1D) (Sanchez-Gurmaches and Guertin, 2014). Thus, Raptor, but not Rictor, is also essential in the *Myf5* lineage for establishing bAPCs during embryogenesis.

Brown and White Adipose Tissue Growth Requires Rictor

Although *Rictor*^{Myf5cKO} mice show no obvious embryonic phenotypes, they tend to weigh less (not significantly) than controls at postnatal day 1 (P1) (Figure S1J), which reaches significance from 6 to 15 weeks of life (Figure 1A). Individual tissue analysis indicates that the weight difference results from decreased adipose tissue mass. For example, the interscapular BAT (iBAT) in

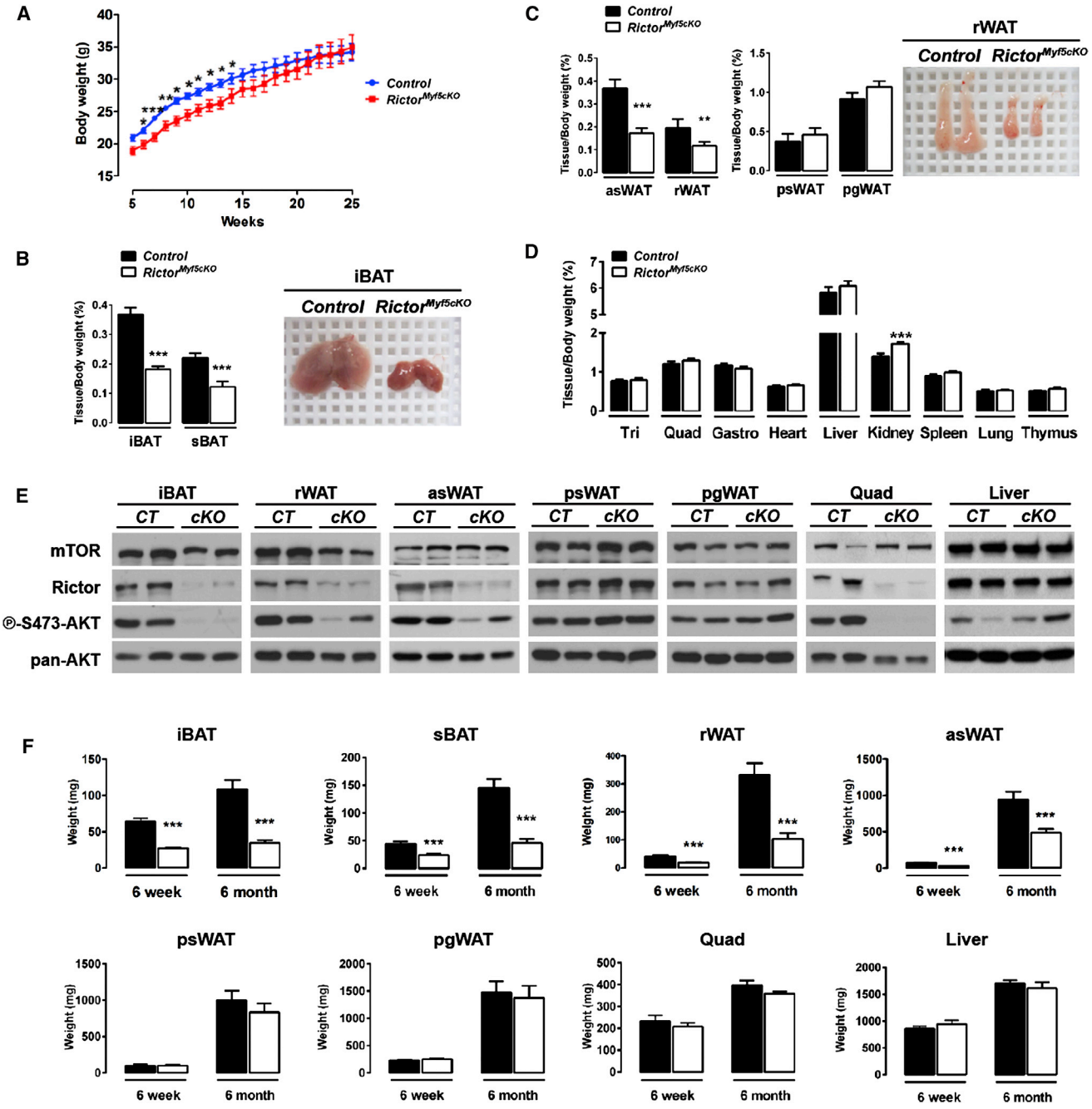

Figure 1. Postnatal Brown and White Adipose Tissue Growth Requires Rictor

(A) Growth curves (n = 13; bars represent mean ± SEM; t test; *p < 0.05, **p < 0.01, ***p < 0.001).

(B) BAT mass at 6 weeks (left) (n = 19–21; mean ± SEM; t test; ***p < 0.001) and representative image (right).

(C) Mass of WATs at 6 weeks (n = 14–16; mean ± SEM; t test; **p < 0.01, ***p < 0.001) (left) and representative image of control and mutant rWAT (6 weeks) (right).

(D) Lean tissue mass at 6 weeks (n = 15–19; mean ± SEM; t test; ***p < 0.001).

(E) Westerns of tissue lysates (6 weeks).

(F) Average tissue mass (mg) at 6 weeks and 6 months (n = 14–21 for 6 weeks; n = 7 for 6 months; mean ± SEM; t test; ***p < 0.001).

See also Figure S1.

P1 *Rictor*^{Myf5cKO} neonates weighs about 30% less than normal (Figure S1K), and during the first weeks of life, the mutant BAT grows but to a much smaller size, resulting in mutant iBAT and subscapular BAT (sBAT) depots at 6 weeks that weigh about 50% less than controls and are darker (Figure 1B). Adipocytes in the retroperitoneal and anterior subcutaneous WAT depots

(rWAT and asWAT, respectively) are also derived largely from *Myf5-Cre*-expressing precursors (Sanchez-Gurmaches and Guertin, 2014; Sanchez-Gurmaches et al., 2012), and both of these depots also decrease in mass by approximately 50% in the $Rictor^{Myf5cKO}$ mice (Figure 1C). In contrast, the posterior subcutaneous and perigonadal WAT depots (psWAT and pgWAT, respectively), which are composed of *Myf5*-negative lineage adipocytes, do not differ in weight (Figure 1C). Skeletal muscles (e.g., triceps, quadriceps, and gastrocnemius) and all other lean tissues examined except the kidneys (which are slightly larger) are of normal size in the KO (Figure 1D). Western analysis for Rictor protein confirms *Rictor* deletion and reduced AKT-S473 phosphorylation in iBAT and muscle and, to a lesser extent, in rWAT and asWAT, but not in psWAT, pgWAT, or liver (Figure 1E).

From 6 weeks to 6 months, the mutant iBAT and sBAT show no additional growth increase, whereas asWAT and rWAT grow to about half (asWAT) or one-third (rWAT) the size of their anatomically matched control tissues (Figure 1F). In contrast, $Rictor^{Myf5cKO}$ psWAT, pgWAT, muscles, and liver grow to their normal size in the same time frame (Figure 1F). Thus, $Rictor^{Myf5cKO}$ mice can grow small BAT tissues in the first weeks of life; however, as $Rictor^{Myf5cKO}$ mice age, the iBAT and sBAT maintain their weight, whereas asWAT and rWAT grow at a reduced rate. Collectively, these results indicate Rictor is essential in the *Myf5* lineage for adipose tissue growth, but not for skeletal muscle growth.

Brown Adipocytes Lacking Rictor Are Smaller

To better define the BAT growth defect, we histologically examined iBAT in control and $Rictor^{Myf5cKO}$ mice. At E18.5, there is no qualitative difference between control and $Rictor^{Myf5cKO}$ bAPCs pools (Figure 2A). In P1 neonates, however, lipids begin accumulating in control BAT, but not in the $Rictor^{Myf5cKO}$ BAT (Figure 2A). From P1 to 6 months, lipid droplets grow in size in control BAT but remain small in the $Rictor^{Myf5cKO}$ BAT (Figure 2A), resulting in smaller cells measured by the increase in nuclei per mm^2 (Figure S2A). Total genomic DNA content is also lower in the $Rictor^{Myf5cKO}$ BAT, indicating additional hypoplasia (Figure S2B). In contrast, $Rictor^{Myf5cKO}$ skeletal muscle fibers appear histologically identical to control fibers (Figure S2C).

Myf5-Lineage White Adipocytes Lacking Rictor Are Also Small and Multilocular

Compared to controls, many adipocytes in the $Rictor^{Myf5cKO}$ rWAT and asWAT are also smaller and multilocular (Figure 2B), but the pattern is heterogeneous in that several large unilocular white adipocytes are also detectable. The psWAT and pgWAT adipocytes appear unchanged in the KO (Figure S2C). The adipocyte precursor pools in rWAT and asWAT are a mix of *Myf5-Cre*-lineage-positive and negative precursors (Sanchez-Gurmaches et al., 2012). Therefore, we reasoned that the size heterogeneity in $Rictor^{Myf5cKO}$ rWAT and asWAT could reflect a mosaic of *Myf5*-lineage-negative (i.e., undeleted) and *Myf5*-lineage-positive (i.e., *Rictor* KO) cells. To test this, we incorporated the *Rosa26-mTmG* reporter (Muzumdar et al., 2007) into control and $Rictor^{Myf5cKO}$ mice to irreversibly label Cre-expressing cells and their lineages with membrane-targeted enhanced GFP (mGFP); all other (Cre^{neg}) cells and their descendants are labeled with membrane-targeted tdTomato fluorescent protein (mTFP). The result is unequivocal; only the small adipocytes are $mGFP^+$ in $Rictor^{Myf5cKO}$ rWAT and asWAT, whereas all the large unilocular adipocytes are $mTFP^+$ (Figure 2C). As expected, in both the control and $Rictor^{Myf5cKO}$ mice, the iBAT adipocytes are $mGFP^+$ and the psWAT and pgWAT adipocytes are $mTFP^+$ (Figure S2D). We also detect a slight increase in UCP1 staining in the $Rictor^{Myf5cKO}$ adipocytes, suggesting the cells might have brown-adipocyte-like characteristics (Figure S2E) (not shown). These data confirm that the heterogeneous small-cell phenotype results from cell-autonomous *Rictor* deletion in the *Myf5*-lineage white adipocytes.

Lipogenesis Is Decreased in Rictor-Deficient BAT

We hypothesized that the paucity of lipid and marked color difference between control and $Rictor^{Myf5cKO}$ BAT indicates a shift from a lipogenic to oxidative state. To test this, we first examined AKT signaling in BAT, which positively regulates lipogenesis. In vivo AKT-T308 phosphorylation is intact in both fasted/refed and insulin-stimulated $Rictor^{Myf5cKO}$ BAT despite ablation of pAKT S473 and pAKT T450 (which is also mTORC2 dependent) (Figures 3A and S3A), consistent with the ability of T-loop (T308) and hydrophobic motif (S473) phosphorylation to be regulated independently (Pearce et al., 2010). Surprisingly, phosphorylation of the AKT substrates FoxO1/3, GSK3β, TSC2, PRAS40, and AS160 is normal in $Rictor^{Myf5cKO}$ BAT (Figure 3A), indicating Rictor is not essential in BAT for pan-AKT signaling. Rictor loss in BAT also does not affect phosphorylation of the SGK substrate NDRG1 (Figure 3A), indicating mTORC2 is not essential for SGK signaling to NDRG1 in BAT or that a compensatory pathway exists.

Next, we examined whether deleting *Rictor* in the *Myf5* lineage affects BAT differentiation markers. In P1 neonates, *Prdm16*, *C/ebpα*, and *C/ebpβ* expression do not differ between controls and KOs, whereas *Pparγ* and *Ucp1* levels slightly decrease (Figure 3B), indicating a possible delay in BAT maturation in the KOs. However, by 6 weeks, *Pparγ*, *Prdm16*, and *C/ebpα* express at control levels, whereas *C/ebpβ*, *Ucp1*, and *Dio2* express at significantly higher-than-control levels (Figure 3B). The mature adipocyte markers *Cidea* and *aP2* are unchanged between control and KO both at P1 and 6 weeks (Figure 3B). Consistent with the gene expression data, PPARγ, UCP1, and insulin receptor beta (IRβ) proteins also express at near-control levels in $Rictor^{Myf5cKO}$ BAT (Figure 3A). Thus, terminal differentiation per se (i.e., PPARγ, UCP1, and IRβ induction) occurs in vivo in $Rictor^{Myf5cKO}$ brown adipocytes.

Next, we examined lipogenesis genes. In P1 $Rictor^{Myf5cKO}$ BAT, acetyl-coA carboxylase (*Acc*), fatty acid synthase (*Fasn*), and fatty acid elongase 6 (*Elovl6*) decrease expression by 40%, 40%, and 25%, respectively (Figure 3C). By 6 weeks, expression of ATP citrate lyase (*Acly*) in addition to *Acc*, *Fasn*, and *Elovl6* is reduced by 90%, 75%, 80%, and 40%, respectively (Figure 3C), which we confirmed by western blot for ACLY and ACC (Figure 3A). In addition, stearoyl-CoA desaturase (*Scd1*) decreases expression by 45% in 6-week $Rictor^{Myf5cKO}$ BAT (Figure 3C). The SREBP1c and ChREBP transcription factors regulate lipogenesis gene expression (Czech et al., 2013; Filhoulaud et al., 2013). In both P1 and 6-week $Rictor^{Myf5cKO}$ BAT, the mRNA

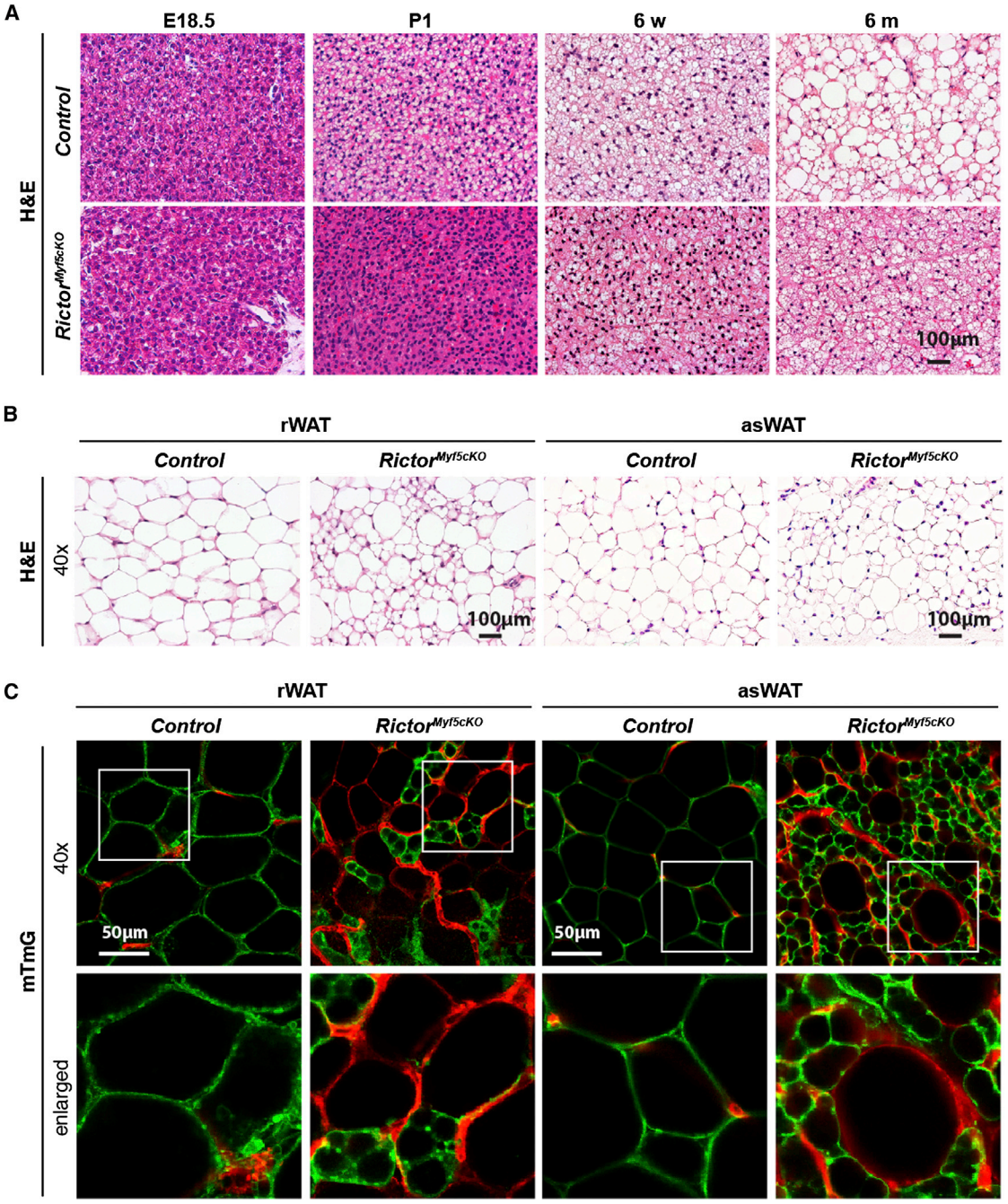

Figure 2. Brown and White Adipocytes Lacking *Rictor* Are Smaller and Multilocular

(A) H&E stains of interscapular BAT (6 weeks).

(B) H&E stains of retroperitoneal and anterior subcutaneous WAT.

(C) Representative images of mTFP- and mGFP-labeled adipocytes. Enlarged images indicated by white box.

See also Figure S2.

expression of SREBP1c (*Srebf1c*), which is induced by insulin, and ChREBP (α and β isoforms), which is induced by glucose, is similar (Figure 3D). However, there is a marked decrease in the amount nuclear SREBP1c (nSREBP1c), the transcriptionally active SREBP1c cleavage product, in Rictor-deficient BAT (Figure 3A) consistent with the decrease in lipogenic gene expression. The levels of *insig1,* another nSREBP1c target gene and negative regulator of SREBP1c processing, also decreases (Figure 3C). The mRNA expression of SREBP2 (which regulates cholesterol biosynthesis) slightly decreases in *Rictor*^{Myf5cKO}

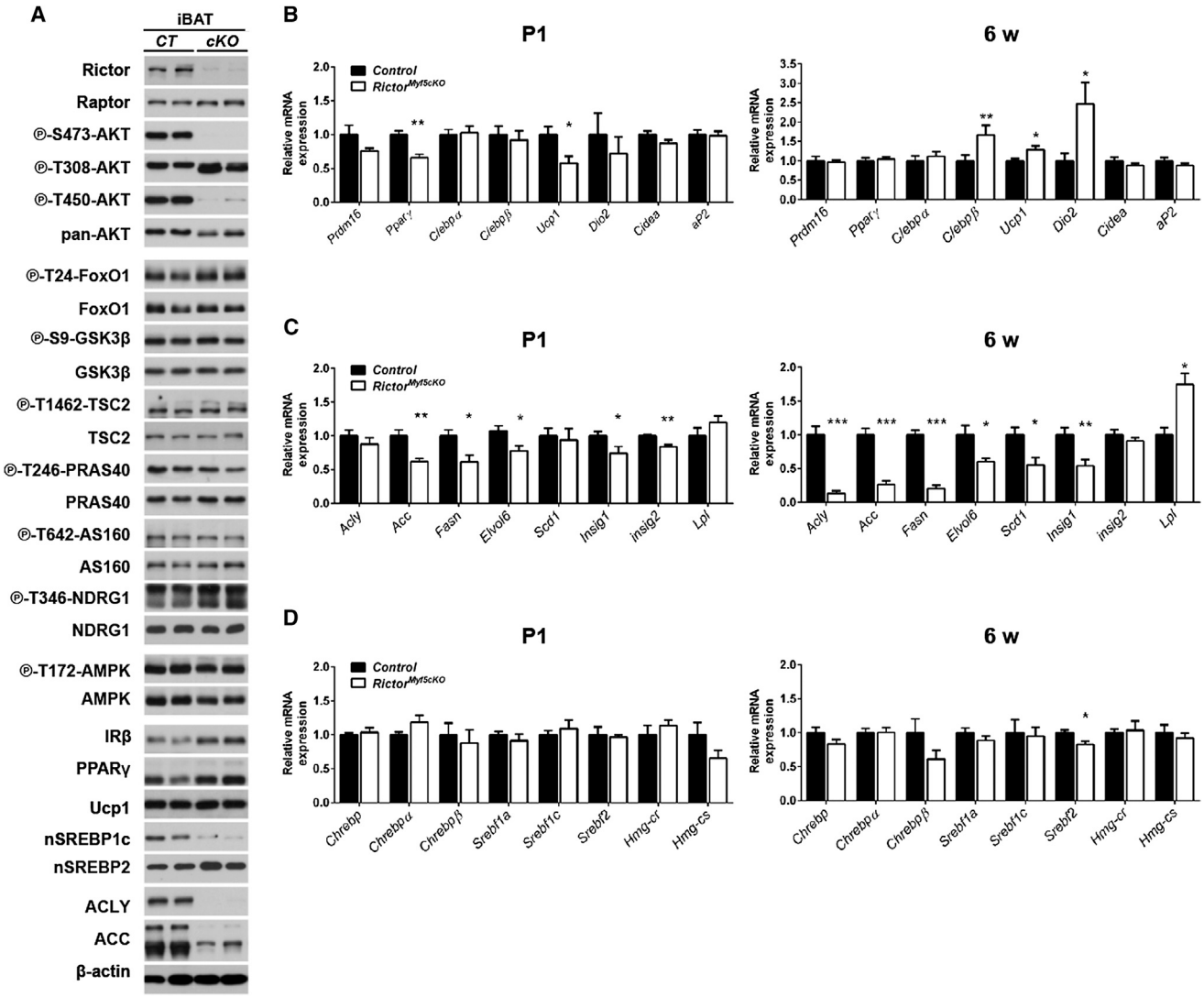

Figure 3. Rictor-Deficient Brown Adipocytes Have a Lipid Metabolism Defect

(A) Western blots total and phosphoproteins using 6-week iBAT lysates. Mice were fasted overnight and refed for 45 min prior to preparing lysates.

(B–D) qRT-PCR of the indicated genes in P1 (n = 6) and 6-week (n = 8) iBAT (mean ± SEM; t test; *p < 0.05, **p < 0.01)

See also Figure S3.

BAT at 6 weeks, but the SREBP2 target genes HMG-CoA synthase (*Hmg-cs)* and HMG-CoA reductase (*Hmg-cr*) express at similar levels in control and KO BAT (Figure 3D), and nuclear SREBP2 (nSREBP2) accumulates possibly to higher levels in the KO BAT (Figure 3A). We find no difference in AMPK or hormone-sensitive lipase phosphorylation between control and *Rictor*^{Myf5cKO} BAT (Figures 3A and S3A). Together, these results indicate that despite having seemingly normal AKT signaling, de novo lipogenesis is reduced in *Rictor*^{Myf5cKO} BAT.

Mitochondrial Activity Is Elevated in Rictor-Deficient BAT

To further examine the metabolic state of *Rictor*^{Myf5cKO} BAT, we examined mitochondrial activity. In P1 neonate *Rictor*^{Myf5cKO} BAT, *Pgc1a* expresses normally, whereas expression of mitochondrial transcription factor A (*Tfam)*, which regulates mtDNA replication, and carnitine palmitoyltransferase 1B *(Cpt1b)*, which encodes the rate-limiting enzyme in β-oxidation, slightly decreases (Figure 4A). In contrast, *Pgc1a*, *Tfam*, and *Cpt1b* in addition to *Ucp1* express at higher levels in the BAT of 6-week-old *Rictor*^{Myf5cKO} mice (Figures 4A and 3B), suggesting BAT mitochondrial activity progressively increases or is maintained at a higher level in *Rictor*^{Myf5cKO} mice as they age.

To explore this in more detail, we used quantitative RT-PCR (qRT-PCR) arrays to broadly measure mitochondrial gene expression in the 6-week-old BAT. Using arrays for functional genes involved in mitochondrial molecular transport and biogenesis, we detect increases in several genes indicative of increased mitochondrial activity (Figure 4B). Furthermore, the mitochondrial citrate and malate transporters *Slc25a1* and *Slc25a10*

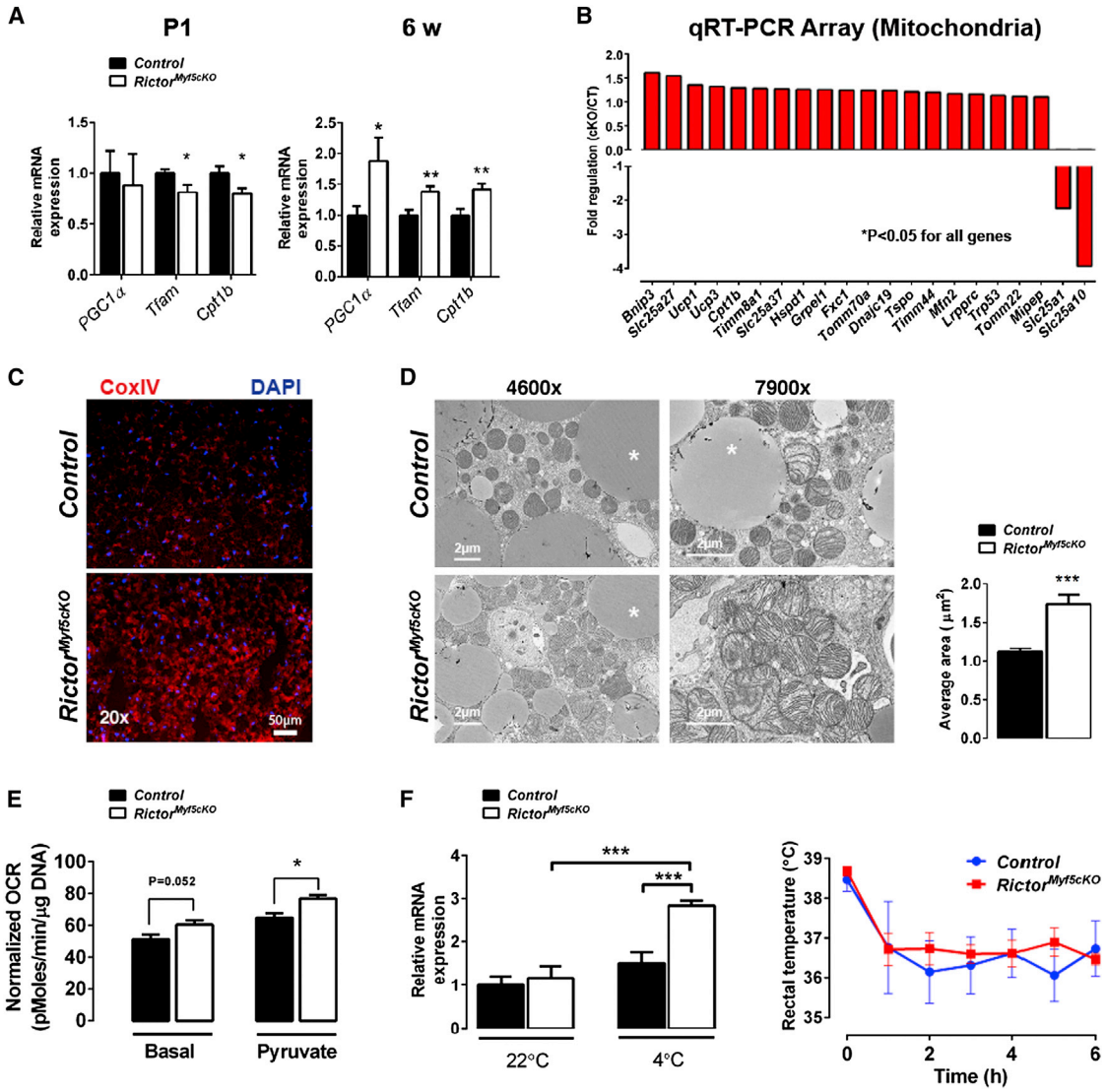

Figure 4. Mitochondrial Activity Is Elevated in Rictor-Deficient BAT

(A) qRT-PCR of mitochondrial genes in P1 (n = 6) and 6-week iBAT (n = 8) (mean ± SEM; t test; *p < 0.05, **p < 0.01)

(B) Differentially expressed genes using mitochondrial qRT-PCR arrays (n = 4; t test; p < 0.05)

(C) Representative immunofluorescence images of Cox IV staining in 6-week iBAT (n = 3).

(D) Representative TEM images of 6-week iBAT (left) and mitochondria size (right) (n = 3; mean ± SEM; t test; ***p < 0.001)

(E) Oxygen consumption of iBAT using a Seahorse Flux Analyzer (12 weeks, n = 5; normalized to DNA content; mean ± SEM; t test; *p < 0.05)

(F) qRT-PCR of *Ucp1* mRNA in iBAT with or without cold exposure (left) (n = 3 for 22°C; n = 4 for 4°C; mean ± SEM; two-way ANOVA; ***p < 0.001) and rectal temperature in acute cold challenge (right) (n = 4; mean ± SEM; t test; no significant difference).

See also Figure S4.

respectively—both of which function in fatty acid biosynthesis, the former also being an SREBP1c target gene (Infantino et al., 2007; Mizuarai et al., 2005)—significantly decrease expression in the mutant BAT. Using mitochondrial energy metabolism gene arrays, we found 58 additional genes involved in respiration (OXPHOS) are elevated in *Rictor*^{Myf5cKO} BAT (Figure S4A), suggesting an increase in mitochondrial mass, which we confirmed by Cox IV immunofluorescence (Figure 4C). Transmission electron microscopy (TEM) reveals individual mitochondria in the mutant BAT are larger and have more disorganized cristae (Figure 4D). To directly confirm elevated mitochondrial activity, we measured BAT oxygen consumption rate (OCR) in a Seahorse Flux Analyzer and determined that basal and pyruvate-stimulated OCRs are elevated by around 18% in *Rictor*^{Myf5cKO} BAT (Figure 4E). We did not detect a significant increase in overall oxygen consumption when *Rictor*^{Myf5cKO} mice were placed in metabolic cages at 22°C, except when normalized for body weight (Figure S4B). Notably, however, mice are under thermal stress at this temperature, which can mask effects on BAT activity (Feldmann et al., 2009).

Interestingly, we also detect an approximate 2-fold increase in basal glucose uptake in *Rictor*^{Myf5cKO} BAT measured by ^{18}FDG positron emission tomography computed tomography scanning (Figure S4C) and an increase in lipoprotein lipase (*Lpl*) expression (Figure 3C), suggesting that *Rictor*^{Myf5cKO} BAT may consume more nutrients than age-matched control BAT. Small-metabolite profiling reveals that *Rictor*^{Myf5cKO} BAT also has elevated levels of inosine monophosphate (IMP) (Figure S4D), a deamination product of AMP, the accumulation of which suggests increased uncoupling (Balcke et al., 2011). In an acute cold challenge, Rictor-deficient BAT also induces *Ucp1* expression significantly more than control BAT and the mutants have no difficulty maintaining body temperature, although body temperature regulation in an acute cold challenge is largely a function of muscle (Figure 4F). Finally, we see no compensatory "browning" in the psWAT as would be expected if *Rictor*^{Myf5cKO} BAT were dysfunctional (Figures S2C and S2D) (Schulz et al., 2013). These results are consistent with Rictor loss in BAT shifting metabolism to a more oxidative and less lipogenic state.

Brown Preadipocytes Require Rictor to Differentiate In Vitro

To examine if brown adipocyte differentiation also requires Rictor in vitro, we generated brown adipocyte precursor cells (bAPCs) harboring an inducible KO system (i.e., *Rictor*^{iKO}) in which *Rictor* deletion is triggered by 4-hydroxytamoxifen (4-OHT) (Figure S5A). Compared to isogenic controls, inducibly deleting *Rictor* rapidly and robustly depletes Rictor protein and AKT-S473 phosphorylation and, consistent with our in vivo data, leaves AKT-T308 phosphorylation intact (Figure S5B). Also consistent with the in vivo results, both basal and insulin-stimulated phosphorylation of FoxO1/3, GSK3β, TSC2, and PRAS40 are normal in *Rictor*^{iKO} bAPCs (Figure 5A). S6K1 phosphorylation is also unaffected (Figure 5A). Contrary to the in vivo results, acute *Rictor* loss in vitro decreases NDRG1 phosphorylation (Figure 5A). This indicates Rictor is required in cultured bAPCs for SGK activity to NDRG1, but not for pan-AKT or mTORC1 activity.

To our surprise, *Rictor*^{iKO} bAPCs are completely incapable of synthesizing lipid droplets when induced to differentiate (Figure 5B). This is surprising, because *Rictor*^{iKO} cells maintain normal levels of pAKT-T308, pGSK3β-S9, and pS6K1-T389 (i.e., PDK1, AKT, and mTORC1 activity, respectively) throughout the differentiation protocol (Figure 5C). The differentiation block occurs early as *Rictor*^{iKO} bAPCs fail to induce *C/ebpα*, *Pparγ*, *Prdm16*, *Pgc1α*, *Srebf1c*, *Ucp1*, and *Glut4* (Figures 5D and S5C). The expression of *C/ebpδ* and *C/ebpβ* on the other hand is induced normally and slightly higher (respectively) in the *Rictor*^{iKO} bAPCs at differentiation day 6 (Figure 5D). Consistent with the gene expression data, PPARγ, IRβ, UCP1, nSREBP1c, ACC, and ACLY levels fail to increase during differentiation in *Rictor*^{iKO} bAPCs (Figure 5E). Notably, 4-OHT or CreER activation alone (i.e., in the absence of *Rictor* floxed alleles) has no effect on differentiation (not shown). Moreover, bAPCs prepared from P1 *Rictor*^{Myf5cKO} neonates also fail to differentiate, indicating that the ex vivo differentiation block is not unique to using the inducible KO system (Figure S5D). Importantly, expressing recombinant PPARγ in *Rictor*^{iKO} bAPCs rescues IRβ, UCP1, and nSREBP1c expression (Figure 5F) and lipid droplet production (Figure 5G), indicating Rictor promotes differentiation at least in part by facilitating PPARγ induction.

Insulin receptor substrate 1 (*Irs1*) and *Irs3* KO bAPCs also fail to induce PPARγ ex vivo (Fasshauer et al., 2001). It was later shown that *Irs1/3* KO bAPCs are unable to differentiate because they express high levels of *Pref-1*, *Wnt10a*, and *Necdin*, which encode adipogenesis inhibitors (Tseng et al., 2005). In contrast, *Rictor*-deficient bAPCs express normal levels of *Pref-1*, *Wnt10a*, and *Necdin* in culture, and during differentiation, *Necdin* and *Pref-1* increase, but only late in the differentiation protocol (Figure S5C). Thus, the mechanism by which deleting *Rictor* inhibits brown adipocyte differentiation differs from that of deleting *Irs1/3*.

AKT1 Functions Downstream of Rictor in Brown Adipocyte Differentiation

To further explore the mechanism by which Rictor regulates differentiation, we next asked whether an AKT or SGK pathway is required downstream of Rictor. To this end, we generated *Rictor*^{iKO} bAPCs that express hemagglutinin (HA)-SGK1, HA-AKT1, and HA-AKT2 or their phosphomimetic counterparts HA-SGK-S422D, HA-AKT1-S473D, and HA-AKT2-S474D in which a phosphomimetic residue was placed at the mTORC2 hydrophobic motif site, confirmed they were functional (Figure S6A), and asked whether any of these constructs rescue differentiation. Only HA-AKT1-S473D efficiently rescues lipid biosynthesis (Figure 6A). HA-AKT1-S473D-expressing *Rictor*^{iKO} bAPCs also induce PPARγ and restore IRβ, UCP1, nSREBP1c, ACLY, and ACC expression (Figure 6B). Thus, Rictor promotes differentiation as part of mTORC2 through an AKT pathway.

Our rescue experiments point to AKT1 as the isoform driving bAPC differentiation in vitro. Consistently, AKT1 is highly expressed in undifferentiated precursors and decreases expression during differentiation, whereas AKT2 expression increases during differentiation (Figure S6B). To further examine the role of AKT1 and AKT2 in bAPC differentiation, we generated bAPC lines that specifically lack either *Akt1* or *Akt2* and determined their in vitro differentiation capacity. Consistent with AKT1, but not AKT2, being required for differentiation, *Akt1*-deficient bAPCs cannot efficiently synthesize lipid droplets (Figure 6C) or upregulate PPARγ, IRβ, or UCP1 when induced to differentiate (Figure 6D). In contrast, *Akt2*-deficient bAPCs induce PPARγ, IRβ, and UCP1 normally (Figures 6C and 6D), indicating that AKT1 is indeed the isoform required downstream of Rictor/mTORC2 for brown adipocyte differentiation. Interestingly, we noticed in our in vitro differentiation assays that although the *Akt2*-deficient cells differentiate, they fail to induce nSREBP1c, that ACLY and ACC express at low levels, and that lipid droplet content is reduced (Figures 6C and 6D). This suggests that although AKT2 is not essential for differentiation, it is important downstream of Rictor/mTORC2 for lipid metabolism. Indeed, when we immunoprecipitate AKT1 or AKT2 from undifferentiated bAPCs, most of the AKT phosphorylation is on AKT1, while in vivo the bulk of AKT phosphorylation shifts to AKT2 (Figures S6C and S6D). Thus, although the inability of *Rictor*^{iKO} bAPCs to differentiate in culture reflects

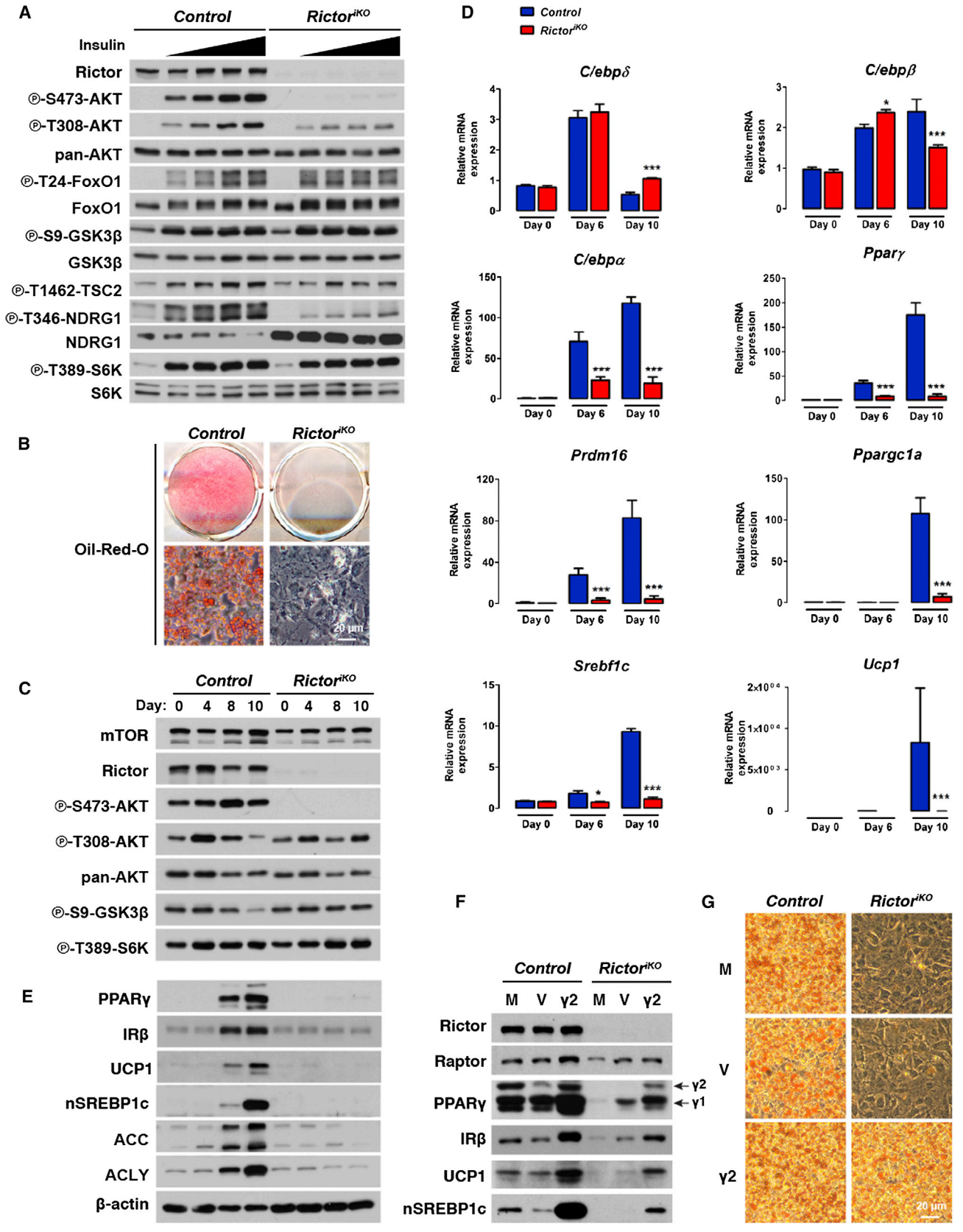

(legend on next page)

an AKT1 deficiency, the in vivo metabolic phenotype appears to reflect an AKT2 deficiency.

BMP7 Rescues Brown Adipocyte Differentiation in the Absence of Rictor

In vitro *Rictor*^{iKO} bAPCs cannot differentiate (i.e., induce PPARγ and UCP1), but in vivo, PPARγ and UCP1-positive Rictor-deficient BAT develops. One possible explanation for this paradox is that in vivo there are developmental signals present that are missing from the artificial in vitro differentiation assay. The signals that drive brown adipocyte differentiation in vivo are poorly understood. One proposed inducer of brown adipocyte differentiation is the transforming growth factor-β superfamily member BMP7 (Schulz and Tseng, 2013; Tseng et al., 2008). When given to control or *Rictor*^{iKO} bAPCs, BMP7 does not induce AKT phosphorylation (Figure S6E). However, when supplemented into the differentiation cocktail, BMP7 restores to *Rictor*^{iKO} bAPCs their ability to synthesize lipid droplets (Figure 6E) and express PPARγ, IRβ, UCP1, and to a lesser extent nSREBP1c, ACLY, and ACC (Figure 6F). This is consistent with the in vitro differentiation assay lacking signaling molecules present in vivo and suggests BMP7 and mTORC2-AKT1 signaling converge during brown adipocyte differentiation. A model depicting the role mTORC2-AKT signaling in vitro in brown adipocyte differentiation is shown in Figure 6G.

Rictor^{Myf5cKO} Mice Are Less Susceptible to Obesity and Metabolic Disease at Thermoneutrality

The higher metabolic activity of Rictor-deficient BAT led us to wonder whether *Rictor*^{Myf5cKO} mice are resistant to obesity. Chronic consumption of a high-fat diet (HFD) triggers a phenomenon in mice called diet-induced thermogenesis, which requires UCP1 and counteracts obesity (Cannon and Nedergaard, 2010; Feldmann et al., 2009). Because BAT activity is masked by chronic thermal stress at 22°C, we conducted the following studies at thermoneutrality (30°C for mice), which exempts mice from thermal stress (Feldmann et al., 2009). When eating a normal chow diet, control and *Rictor*^{Myf5cKO} mice gain equal weight (Figure 7A) and consume the same total energy (Figure 7B) over 12 weeks. In contrast, when eating an HFD, control mice gain 14.67 ± 1.05 g whereas *Rictor*^{Myf5cKO} mice gain 10.57 ± 1.18 g (Figure 7A), despite both groups consuming the same energy (Figure 7B). Thus, controls gain 64% more weight when eating an HFD versus chow compared to *Rictor*^{Myf5cKO} mice. This suggests *Rictor*^{Myf5cKO} mice living at thermoneutrality and eating an HFD are less metabolically efficient than controls, which is indeed the case (Figure 7C).

The resistance to weight gain in the HFD-fed *Rictor*^{Myf5cKO} cohort is partly due to reduced growth of adipose tissue. For example, the pgWAT gains significantly less mass in the HFD-fed *Rictor*^{Myf5cKO} cohort than in HFD-fed controls (Figure 7D). Liver and heart also grow larger in controls eating HFD compared to chow, whereas liver and heart grow to the same mass in the *Rictor*^{Myf5cKO} cohorts regardless of diet (Figures 7D and S7A). Diet has no effect on other lean tissues in either the controls or *Rictor*^{Myf5cKO} cohorts (Figures 7D and S7A). That pgWAT grows less in HFD-fed *Rictor*^{Myf5cKO} mice compared to HFD-fed controls indicates systemic protection against obesity is occurring because *Myf5*-Cre does not target pgWAT (Figures 1F and S2C). The reduction in pgWAT mass is due in part to smaller adipocyte size (Figure 7E); the livers of *Rictor*^{Myf5cKO} mice also resist hepatic steatosis (Figure 7E), and the HFD-fed *Rictor*^{Myf5cKO} mice perform better in a glucose tolerance test (Figure S7B).

In chow-fed cohorts, histology reveals that control BAT adopts a more "white adipocyte-like" appearance (Figure 7E). In contrast, the BAT in chow-fed *Rictor*^{Myf5cKO} mice resists the whitening effects of living at thermoneutrality and maintains a more "brown-adipocyte-like" appearance (Figure 7E). The resistance of *Rictor*^{Myf5cKO} BAT to whitening is reflected in the gene expression signature; for example, when normalized to BAT gene expression at 22°C, the shift to thermoneutrality decreases the expression of BAT-selective genes (*Prdm16*, *Sgk2*, *cideb*, and *cyp2b10*) and increases the expression of WAT-selective genes (*Dpt1*, *Retn*, *Trim14*, and *Nnmt*) (Harms et al., 2014) to a greater extent in control BAT than in *Rictor*^{Myf5cKO} BAT, which maintains a more BAT-like identity (Figure S7C).

In HFD-fed cohorts, histology reveals a large number of multilocular adipocytes in control BAT (Figure 7F) that are not apparent in chow-fed controls (Figure 7E), suggesting diet-induced thermogenesis. This is reflected in the gene expression data as *Prdm16* increases in control BAT in HFD-fed mice compared to chow-fed mice (Figure 7G), whereas the WAT-specific genes *Retn*, *Trim14*, and *Nnmt* decrease (Figure 7G). Histology also reveals that *Rictor*^{Myf5cKO} BAT is even more "brown-like" in the HFD-fed cohort, exhibiting a uniform abundance of small lipid droplets (Figure 7F) and a stronger BAT gene signature (i.e., elevated *Prdm16*, *Sgk2*, *Cideb*, and *Cyp2b10* and decreased *Dpt1*, *Retn*, *Trim14*, and *Nnmt*) (Figure 7G). Consistently, BAT functional genes (*Ucp1*, *Pgc1α*, *Cpt1β*, and *Dio2*) are induced to a greater extent in HFD-fed *Rictor*^{Myf5cKO} mice (Figure 7H), which also maintain low *Acly*, *Acc*, and *Fasn* expression (Figure S7D). Importantly, UCP1 protein levels are higher in the BAT of *Rictor*^{Myf5cKO} mice eating an

Figure 5. Rictor Is Required for Brown Adipocyte Differentiation In Vitro

(A) Western immunoblots using control and *Rictor*^{iKO} brown preadipocyte lysates. Cells were serum deprived 3 hr then stimulated with 0, 5, 25, 120, or 600 nM insulin for 15 min prior to lysis.

(B) Oil red O staining after differentiation.

(C) Western immunoblots using lysates from the indicated days of differentiation.

(D) qRT-PCR for differentiation-related genes (n = 3; mean ± SEM; t test; *p < 0.05, ***p < 0.001).

(E) Same as (C).

(F) Western immunoblots of cell lysates collected at day 10 of differentiation. M, mock; V, empty vector; γ2, recombinant PPARγ2. The γ1 and γ2 isoforms are indicated.

(G) Oil red O staining of cells in (F).

See also Figure S5.

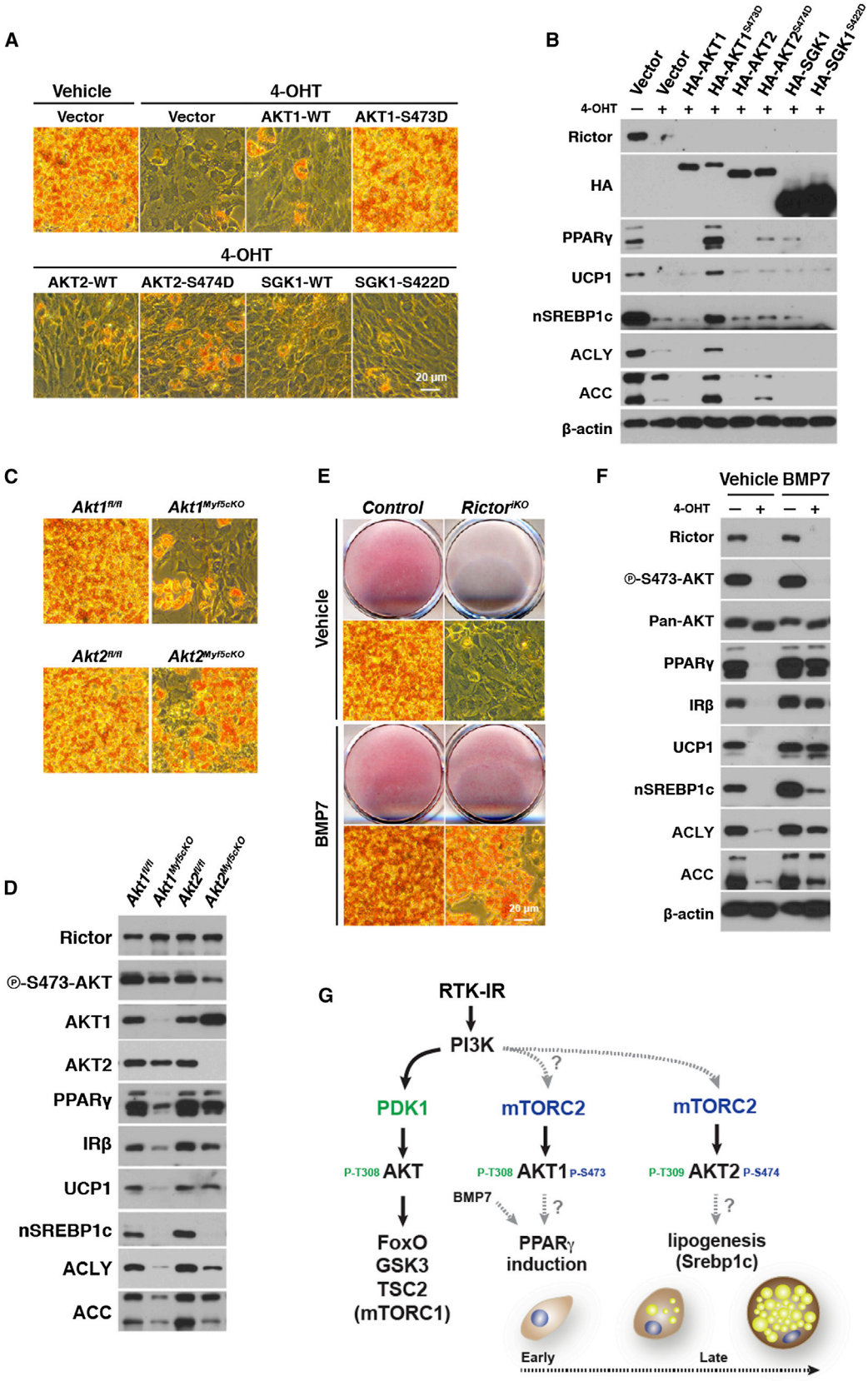

(legend on next page)

HFD (Figure 7I). Notably, after 20 weeks of eating an HFD, the control BAT reverts to a more white-adipocyte-like histology; however, BAT character is preserved in *Rictor*^{Myf5cKO} mice (Figure S7E). Collectively, these results suggest that inhibiting mTORC2 in BAT increases diet-induced thermogenesis and, consequently, *Rictor*^{Myf5cKO} mice living without thermal stress and consuming an obesogenic diet are less susceptible to developing obesity and metabolic disease.

DISCUSSION

Transcriptional regulation of BAT development has been extensively described (Kajimura et al., 2010), whereas less is known about the signaling mechanisms that regulate BAT. The control of brown fat fuel utilization is also incompletely understood (Townsend and Tseng, 2014). Previous studies reported that conditionally deleting *Rictor* in WAT and BAT or skeletal muscle has no affect on WAT or BAT mass or individual adipocyte or myocyte size (Bentzinger et al., 2008; Cybulski et al., 2009; Kumar et al., 2008, 2010). However, these studies used Cre drivers that reportedly delete *Rictor* in mature cells, which led us to hypothesize that Rictor/mTORC2 may be more important for BAT/WAT and/or muscle development. By conditionally deleting *Rictor* in *Myf5* precursors, we discovered that Rictor is not essential in vivo for muscle development or regeneration. In contrast, *Myf5*-lineage brown and white adipocytes lacking Rictor are reduced in size. Furthermore, Rictor-deficient BAT undergoes a metabolic shift to a more oxidative and less lipogenic metabolic despite having seemingly normal pan-AKT signaling. Importantly, at thermoneutrality, this protects mice against an obesogenic diet. These findings implicate Rictor/mTORC2 as an essential signaling node in BAT that regulates the balance between fatty acid oxidation and storage. These findings could have important implications for understanding the signaling mechanisms that regulate fuel usage and metabolic activity in human BAT.

We also report that in vitro brown adipocyte differentiation requires Rictor/mTORC2. Mechanistically, Rictor/mTORC2 promotes *Pparγ* induction through AKT1 independently of pan-AKT signaling and mTORC1 activity. In vivo, however, brown adipocytes differentiate in *Rictor*^{Myf5cKO} mice despite lacking Rictor expression. We hypothesize that this paradox indicates that the artificial in vitro culture conditions lack important signals present in vivo that overcome this deficiency. Supporting this notion, supplementing the differentiation assay with BMP7, a proposed in vivo inducer of brown adipocyte differentiation and thermogenesis (Schulz and Tseng, 2013; Tseng et al., 2008), rescues differentiation in the absence of Rictor. Notably, we do detect low *pparγ* expression in *Rictor*^{Myf5cKO} P1 BAT, which may reflect the role of Rictor/mTORC2 in early brown adipocyte differentiation and explain the mutant BAT hypoplasia. Exactly how Rictor/mTORC2 and BMP7 signaling might converge on PPARγ is not yet clear. We also show that during brown adipocyte differentiation, the major AKT isoform switches from AKT1 to AKT2; thus, although Rictor/mTORC2 may regulate differentiation through an AKT1 pathway that can be bypassed in vivo, its role in BAT metabolism is likely mediated through an AKT2 pathway that cannot be compensated for. Consistent with this idea, whole-body *Akt2* KO mice among many other phenotypes have smaller BATs (Cho et al., 2001; Garofalo et al., 2003).

Why does deleting *Rictor* in BAT cause a metabolic shift? One possibility is that forkhead box O (FOXO) transcription factors are more active in Rictor-deficient brown adipocytes. FOXOs are regulated by multiple signals and function as cellular homeostasis regulators under stressful conditions (Eijkelenboom and Burgering, 2013). FoxO1 and FoxO3 are AKT substrates that are partially dephosphorylated in some Rictor-deficient cells (Guertin et al., 2006, 2009; Hagiwara et al., 2012; Jacinto et al., 2006; Yuan et al., 2012). When dephosphorylated, FoxO1/3 translocate to the nucleus, where they affect metabolism, survival, and cell-cycle genes and the activity of transcriptional regulators (including PPARγ and C/EBPα) (Eijkelenboom and Burgering, 2013). However, FoxO1/3 phosphorylation is not affected in Rictor-deficient BAT; thus, if the metabolic shift is driven by FoxO1/3, it may be through an alterative mechanism such as acetylation (Banks et al., 2011; Masui et al., 2013). Another possibility is that FoxC2 mediates the metabolic shift (Cederberg et al., 2001; Yao et al., 2013); however, we do not observe any change in FoxC2 expression in *Rictor*-deficient preadipocytes (not shown), nor do we see effects on the FoxC2 targets *C/ebpβ* or *Wnt10b* during differentiation (Gerin et al., 2009). The shift could also be mediated through unidentified AKT substrates that uniquely require hydrophobic motif phosphorylation. This is an important ongoing area of investigation.

Consistent with the *Myf5* lineage giving rise to a subset of white adipocytes, we also uncovered an essential role for Rictor/mTORC2 in white adipocyte growth in vivo. This confirms our previous discovery that some white adipocytes arise from *Myf5-Cre* expressing precursors (Sanchez-Gurmaches and Guertin, 2014; Sanchez-Gurmaches et al., 2012). However, because in the *Rictor*^{Myf5cKO} mice the Rictor-deficient white adipocytes are interspersed heterogeneously with nondeleted adipocytes within the same depot, we could not perform the appropriate whole-tissue biochemical studies using Rictor-deficient WAT. We did, however, determine that *Rictor*^{iKO} white adipocyte precursors purified from the stromal vascular fraction of psWAT (which are not *Myf5*-lineage derived) are also defective at differentiating in vitro (not shown), indicating Rictor also has a

Figure 6. Recombinant AKT1-S473D or BMP7 Supplementation Rescue Differentiation in the Absence of Rictor

(A) Oil red O staining of differentiated control (vehicle) and *Rictor*^{iKO} cells (4-OHT) cells stably expressing the indicated constructs.

(B) Western immunoblots corresponding to (A).

(C) Oil red O staining of differentiated *Akt1* and *Akt2* conditional knockout and control bAPCs.

(D) Western immunoblots corresponding to (C).

(E) Oil red O staining of differentiated control and *Rictor*^{iKO} cells in the presence or absence of BMP7 (3.2 nM added day 1 during differentiation).

(F) Western immunoblots of corresponding to (E).

(G) Model summarizing the role of mTORC2 in vitro in brown adipocyte differentiation.

See also Figure S6.

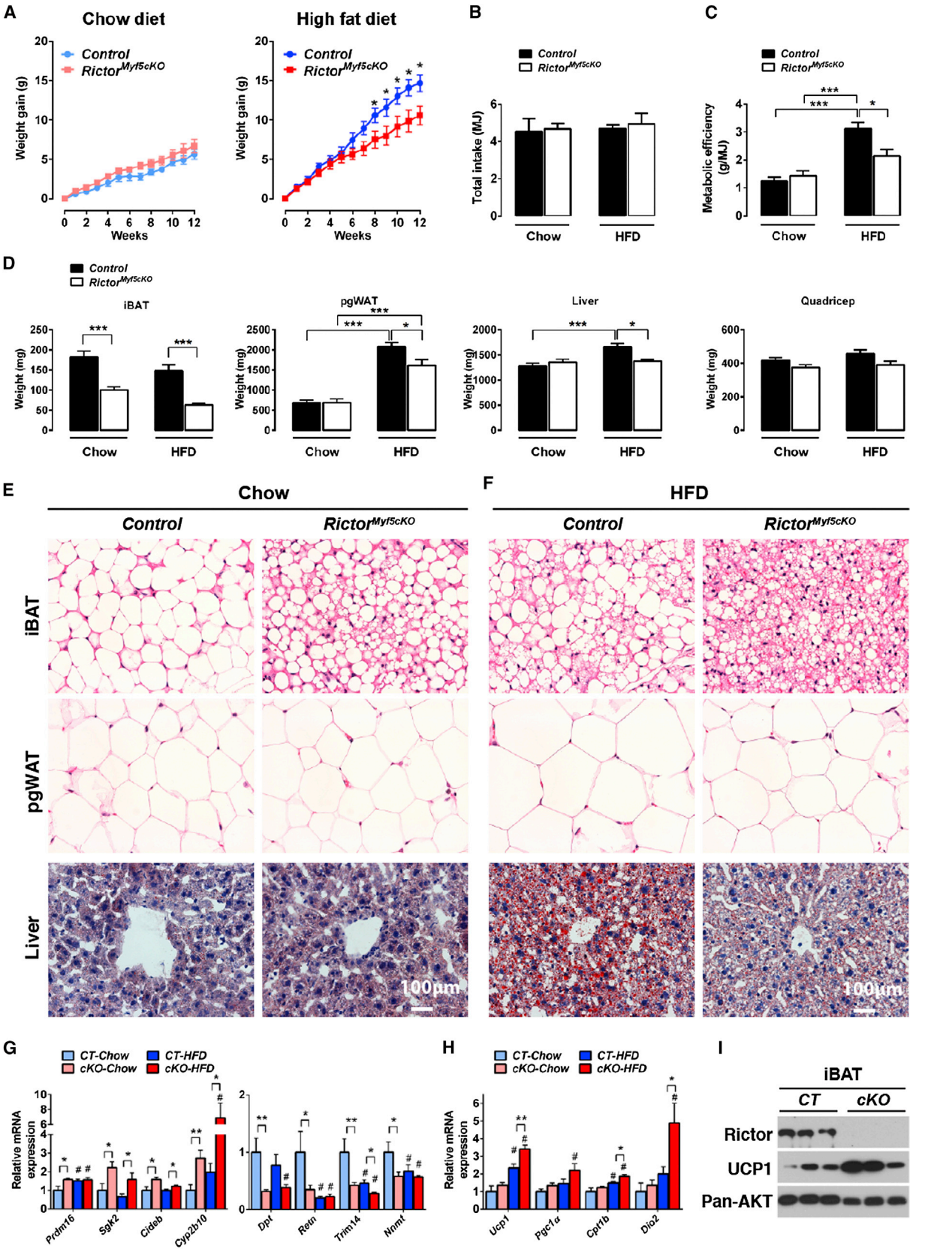

(legend on next page)

cell-autonomous role in white adipocyte differentiation that is not dependent upon being *Myf5*-lineage derived. To determine the in vivo relevance of these findings, we will need to identify Cre drivers that express uniformly and specifically in white adipocyte precursors; however, the origins of adipocytes are just beginning to be revealed, and appropriate tools are not yet available for this line of investigation.

Is Rictor/mTORC2 a master regulator of lipid metabolism? Recent studies of liver collectively report that deleting hepatic *Rictor* results in a complex phenotype including increased gluconeogenesis, decreased glycolysis, and impaired lipogenesis (Hagiwara et al., 2012; Lamming et al., 2012; Yuan et al., 2012). Two studies find that hepatic *Rictor* loss also decreases SREBP1c activity; however, one study suggests AKT2 mediates this function (Hagiwara et al., 2012), whereas the other proposes an AKT-independent pathway (Yuan et al., 2012). These two studies are also inconsistent with respect to how *Rictor* loss affects AKT signaling, and thus the role of hepatic Rictor/mTORC2 is currently controversial. Nevertheless, the glucose uptake and glycolysis defect is reportedly independent of the lipogenesis defect, because restoring glucose flux in *Rictor*-KO hepatocytes did not rescue lipogenesis (Hagiwara et al., 2012). This study also reports that fatty acid oxidation genes are elevated in Rictor-deficient hepatocytes (Hagiwara et al., 2012). Thus, Rictor/mTORC2 may have a broad role in establishing a prolipogenic metabolic state. Going forward, it is important to determine if Rictor/mTORC2 regulates de novo lipogenesis and β-oxidation by a common or coordinate set of mechanisms or whether one metabolic deficiency is indirectly driving the other. Notably, we detect a decrease in lipogenesis gene expression in P1 BAT lacking Rictor, but the increase in fatty acid oxidation gene expression we first detect in 6-week mutant BAT. Thus, mitochondrial activity may progressively increase in the Rictor-deficient BAT and be secondary to a lipogenesis defect. Regardless, our findings support the idea that targeting lipogenesis and/or β-oxidation pathways in adipocytes could be one approach to treating obesity and diabetes.

One prediction is that increasing BAT energy expenditure could have antiobesity therapeutic potential (Tseng et al., 2010). To achieve this goal, a deeper understanding of how BAT utilizes fuel is required (Townsend and Tseng, 2014). An important finding in our study is that $Rictor^{Myf5cKO}$ mice living at thermoneutrality, when challenged with an obesogenic diet, induce higher levels of UCP1 and are more resistant to developing obesity and metabolic disease compared to HFD-fed controls. This suggests that inhibiting mTORC2 in BAT augments diet-induced thermogenesis (Cannon and Nedergaard, 2010; Feldmann et al., 2009), although we cannot yet rule out that Rictor loss in other *Myf5*-lineage tissues might also contribute to this phenotype. It is currently being debated whether humans have classic brown adipocytes or a potential third class of adipocyte called a brite/beige adipocyte (Nedergaard and Cannon, 2013). Recent work indicates that in the neck, deep fat is similar to rodent BAT and expresses high levels of UCP1, whereas more superficial fat expresses lower UCP1 levels and has more brite/beige characteristics (Cypess et al., 2013). Notably, humans typically adjust temperature to be around thermoneutrality (Cannon and Nedergaard, 2010), and the BAT of mice living at thermoneutrality appears more "white-fat like," or perhaps more "brite/beige-fat" like (Figure 7). Thus, it seems likely that humans possess classic brown fat and that studies of brown fat in mice will provide important insights into human BAT regulation. Continued elucidation of mTORC2 pathways in BAT bioenergetics could therefore lead to novel antiobesity therapies that target cellular energy expenditure.

EXPERIMENTAL PROCEDURES

Gene Expression

Total RNA was isolated using Qiazol (Invitrogen) and an RNeasy kit (Invitrogen). Equal amounts of RNA were retrotranscribed to cDNA using a high-capacity cDNA reverse transcription kit (Applied Biosystems). *Tbp* expression was used as a normalization gene. A different set of iBAT samples was used in RT-PCR arrays (QIAGEN) according to the manufacturer's instruction. See also Supplemental Experimental Procedures.

In Vitro Differentiation

Primary brown adipocyte precursor (bAPC) cells were isolated from P1 neonates and immortalized with pBabe-SV40 large T antigen. To induce *Rictor* deletion, *ubc-creERT2;*$Rictor^{fl/fl}$ cells were treated on 3 consecutive days with 1 μM 4-OHT. bAPCs were seeded at 4×10^4 cells/ml and allowed reach confluence over 3 days in medium containing 20 nM insulin and 1 nM T3 (differentiation medium). On day 4, cells were induced with 20 nM insulin, 1nM T3, 0.125 mM indomethacin, 2 μg/ml dexamethasone, and 0.5 mM 3-isobutyl-1-methylxanthine. Two days later, the induction medium was replaced with fresh

Figure 7. $Rictor^{Myf5cKO}$ Mice Exempt from Thermal Stress and Consuming a High-Fat Diet Are Resistant to Obesity and Metabolic Disease

(A) Weight gain of control and $Rictor^{Myf5cKO}$ mice during 12-weeks of normal chow (chow) or high-fat diet (HFD) (n = 8 control and n = 12 for KO in chow; n = 10 for both genotypes on an HFD; mean ± SEM; t test; *p < 0.05). Control mice initially weighed 21.63 ± 0.812 g in the chow group and 21.24 ± 0.621 in the HFD group. The $Rictor^{Myf5cKO}$ mice initially weighed 19.42 ± 0.305 g in the chow group and 19.32 ± 0.348 in the HFD group.

(B) Total energy intake (MJ) during the feeding regimen in (A). Control mice consumed 3.75 ± 0.56 g of chow and 2.81 ± 0.12 g of HFD; $Rictor^{Myf5cKO}$ mice consumed 3.85 ± 0.24 g of chow and 2.95 ± 0.35 g of HFD.

(C) Metabolic efficiency determined as the amount of body weight increase (g) per MJ food consumed (n = 8 control and n = 12 KO on chow; n = 10 for both genotypes on HFD; mean ± SEM; two-way ANOVA; *p < 0.05, ***p < 0.001).

(D) Mass (mg) of the indicated tissues collected from control and KO mice after 12 weeks on chow or an HFD (n = 8 control and n = 12 KO on chow; n = 10 for both genotypes on HFD; mean ± SEM; two-way ANOVA; *p < 0.05, ***p < 0.001).

(E and F) H&E staining of iBAT and pgWAT and oil red O staining of livers after 12 weeks of eating chow (E) or and HFD (F).

(G) qRT-PCR of the indicated brown and white fat genes in iBAT from chow- or HFD-mice (n = 8 control and n = 12 KO on chow; n = 10 for both genotypes on HFD; mean ± SEM; two-way ANOVA; *p < 0.05, **p < 0.01, ***p < 0.001; # indicates significant difference over the control chow group).

(H) qRT-PCR of the indicated metabolic genes in iBAT from chow- or HFD-mice (n = 8 control and n = 12 KO in chow; n = 10 for both genotypes in HFD; mean ± SEM; two-way ANOVA; *p < 0.05, **p < 0.01, ***p < 0.001; # indicates a significant difference over the control chow group).

(I) Western immunoblots of iBAT lysates.

See also Figure S7.

differentiation medium and changed every 2 days until day 10. See also Supplemental Experimental Procedures.

Metabolic Studies

For thermoneutrality studies, 6-week-old male mice were transferred to 30°C. At 7 weeks of age, mice were fed chow (Prolab Isopro RMH3000, LabDiet) or a high-fat diet (45% calories from fat; ResearchDiet # D12451). Body weight and food intake were accessed weekly for 12 weeks. Glucose tolerance tests were performed at the 11th week. Overnight fasted animals were subjected to GTT by intraperitoneally injecting glucose at 2 g/kg of body weight, and blood glucose levels were measured with a commercially available glucose meter. A small group (n = 4) of mice were kept for 20 weeks on an HFD for morphological studies. All animal experiments were approved by the University of Massachusetts Medical school animal care and use committee.

Statistics

Unless otherwise stated, the results are described as mean ± SEM. Two-way ANOVA was performed where indicated. For most experiments, the Student's t test was used to determine statistical significance (*$p < 0.05$; **$p < 0.01$; ***$p < 0.001$).

See also Supplemental Experimental Procedures.

SUPPLEMENTAL INFORMATION

Supplemental Information includes Supplemental Experimental Procedures and seven figures and can be found with this article online at http://dx.doi.org/10.1016/j.celrep.2014.06.007.

AUTHOR CONTRIBUTIONS

C.-M.H. and D.A.G. designed the project and wrote and edited the manuscript. C.-M.H. performed most experiments, and D.A.G. assisted in analysis and interpretation. C.M.C., J.S.-G., and H.L. assisted with rescue, lineage tracing, and mouse experiments. C.B.C. performed metabolite profiling. S.H. and A.J.W. assisted with muscle experiments.

ACKNOWLEDGMENTS

This work was supported by grants from the NIH (R00CA129613 and R01DK094004), the American Diabetes Association (ADA113BS-066), the Pew Charitable Trusts, and the Charles Hood Foundation (to D.A.G.). We thank Yuefeng Tang, Xiaohao Yao, and Christine Powers for technical assistance, Morris Birnbaum for *Akt* floxed mice, and Marcus Cooper for the PPARγ2 construct. Metabolic cage studies were performed in the UMass Mouse Phenotype Center (DK09300).

Received: October 31, 2013
Revised: April 30, 2014
Accepted: June 4, 2014
Published: July 3, 2014

REFERENCES

Balcke, G.U., Kolle, S.N., Kamp, H., Bethan, B., Looser, R., Wagner, S., Landsiedel, R., and van Ravenzwaay, B. (2011). Linking energy metabolism to dysfunctions in mitochondrial respiration—a metabolomics in vitro approach. Toxicol. Lett. *203*, 200–209.

Banks, A.S., Kim-Muller, J.Y., Mastracci, T.L., Kofler, N.M., Qiang, L., Haeusler, R.A., Jurczak, M.J., Laznik, D., Heinrich, G., Samuel, V.T., et al. (2011). Dissociation of the glucose and lipid regulatory functions of FoxO1 by targeted knockin of acetylation-defective alleles in mice. Cell Metab. *14*, 587–597.

Bentzinger, C.F., Romanino, K., Cloëtta, D., Lin, S., Mascarenhas, J.B., Oliveri, F., Xia, J., Casanova, E., Costa, C.F., Brink, M., et al. (2008). Skeletal muscle-specific ablation of raptor, but not of rictor, causes metabolic changes and results in muscle dystrophy. Cell Metab. *8*, 411–424.

Cannon, B., and Nedergaard, J. (2004). Brown adipose tissue: function and physiological significance. Physiol. Rev. *84*, 277–359.

Cannon, B., and Nedergaard, J. (2010). Metabolic consequences of the presence or absence of the thermogenic capacity of brown adipose tissue in mice (and probably in humans). Int. J. Obes. (Lond.) *34* (*Suppl 1*), S7–S16.

Cederberg, A., Grønning, L.M., Ahrén, B., Taskén, K., Carlsson, P., and Enerbäck, S. (2001). FOXC2 is a winged helix gene that counteracts obesity, hypertriglyceridemia, and diet-induced insulin resistance. Cell *106*, 563–573.

Cho, H., Mu, J., Kim, J.K., Thorvaldsen, J.L., Chu, Q., Crenshaw, E.B., 3rd, Kaestner, K.H., Bartolomei, M.S., Shulman, G.I., and Birnbaum, M.J. (2001). Insulin resistance and a diabetes mellitus-like syndrome in mice lacking the protein kinase Akt2 (PKB beta). Science *292*, 1728–1731.

Cybulski, N., Polak, P., Auwerx, J., Rüegg, M.A., and Hall, M.N. (2009). mTOR complex 2 in adipose tissue negatively controls whole-body growth. Proc. Natl. Acad. Sci. USA *106*, 9902–9907.

Cypess, A.M., White, A.P., Vernochet, C., Schulz, T.J., Xue, R., Sass, C.A., Huang, T.L., Roberts-Toler, C., Weiner, L.S., Sze, C., et al. (2013). Anatomical localization, gene expression profiling and functional characterization of adult human neck brown fat. Nat. Med. *19*, 635–639.

Czech, M.P., Tencerova, M., Pedersen, D.J., and Aouadi, M. (2013). Insulin signalling mechanisms for triacylglycerol storage. Diabetologia *56*, 949–964.

Eijkelenboom, A., and Burgering, B.M. (2013). FOXOs: signalling integrators for homeostasis maintenance. Nat. Rev. Mol. Cell Biol. *14*, 83–97.

Fasshauer, M., Klein, J., Kriauciunas, K.M., Ueki, K., Benito, M., and Kahn, C.R. (2001). Essential role of insulin receptor substrate 1 in differentiation of brown adipocytes. Mol. Cell. Biol. *21*, 319–329.

Feldmann, H.M., Golozoubova, V., Cannon, B., and Nedergaard, J. (2009). UCP1 ablation induces obesity and abolishes diet-induced thermogenesis in mice exempt from thermal stress by living at thermoneutrality. Cell Metab. *9*, 203–209.

Filhoulaud, G., Guilmeau, S., Dentin, R., Girard, J., and Postic, C. (2013). Novel insights into ChREBP regulation and function. Trends Endocrinol. Metab. *24*, 257–268.

García-Martínez, J.M., and Alessi, D.R. (2008). mTOR complex 2 (mTORC2) controls hydrophobic motif phosphorylation and activation of serum- and glucocorticoid-induced protein kinase 1 (SGK1). Biochem. J. *416*, 375–385.

Garofalo, R.S., Orena, S.J., Rafidi, K., Torchia, A.J., Stock, J.L., Hildebrandt, A.L., Coskran, T., Black, S.C., Brees, D.J., Wicks, J.R., et al. (2003). Severe diabetes, age-dependent loss of adipose tissue, and mild growth deficiency in mice lacking Akt2/PKB beta. J. Clin. Invest. *112*, 197–208.

Gerin, I., Bommer, G.T., Lidell, M.E., Cederberg, A., Enerback, S., and Macdougald, O.A. (2009). On the role of FOX transcription factors in adipocyte differentiation and insulin-stimulated glucose uptake. J. Biol. Chem. *284*, 10755–10763.

Gesta, S., Tseng, Y.H., and Kahn, C.R. (2007). Developmental origin of fat: tracking obesity to its source. Cell *131*, 242–256.

Guertin, D.A., Stevens, D.M., Thoreen, C.C., Burds, A.A., Kalaany, N.Y., Moffat, J., Brown, M., Fitzgerald, K.J., and Sabatini, D.M. (2006). Ablation in mice of the mTORC components raptor, rictor, or mLST8 reveals that mTORC2 is required for signaling to Akt-FOXO and PKCalpha, but not S6K1. Dev. Cell *11*, 859–871.

Guertin, D.A., Stevens, D.M., Saitoh, M., Kinkel, S., Crosby, K., Sheen, J.H., Mullholland, D.J., Magnuson, M.A., Wu, H., and Sabatini, D.M. (2009). mTOR complex 2 is required for the development of prostate cancer induced by Pten loss in mice. Cancer Cell *15*, 148–159.

Hagiwara, A., Cornu, M., Cybulski, N., Polak, P., Betz, C., Trapani, F., Terracciano, L., Heim, M.H., Rüegg, M.A., and Hall, M.N. (2012). Hepatic mTORC2 activates glycolysis and lipogenesis through Akt, glucokinase, and SREBP1c. Cell Metab. *15*, 725–738.

Harms, M., and Seale, P. (2013). Brown and beige fat: development, function and therapeutic potential. Nat. Med. *19*, 1252–1263.

Harms, M.J., Ishibashi, J., Wang, W., Lim, H.W., Goyama, S., Sato, T., Kurokawa, M., Won, K.J., and Seale, P. (2014). Prdm16 is required for the

maintenance of brown adipocyte identity and function in adult mice. Cell Metab. *19*, 593–604.

Infantino, V., Iacobazzi, V., De Santis, F., Mastrapasqua, M., and Palmieri, F. (2007). Transcription of the mitochondrial citrate carrier gene: role of SREBP-1, upregulation by insulin and downregulation by PUFA. Biochem. Biophys. Res. Commun. *356*, 249–254.

Jacinto, E., Facchinetti, V., Liu, D., Soto, N., Wei, S., Jung, S.Y., Huang, Q., Qin, J., and Su, B. (2006). SIN1/MIP1 maintains rictor-mTOR complex integrity and regulates Akt phosphorylation and substrate specificity. Cell *127*, 125–137.

Kajimura, S., Seale, P., and Spiegelman, B.M. (2010). Transcriptional control of brown fat development. Cell Metab. *11*, 257–262.

Kumar, A., Harris, T.E., Keller, S.R., Choi, K.M., Magnuson, M.A., and Lawrence, J.C., Jr. (2008). Muscle-specific deletion of rictor impairs insulin-stimulated glucose transport and enhances Basal glycogen synthase activity. Mol. Cell. Biol. *28*, 61–70.

Kumar, A., Lawrence, J.C., Jr., Jung, D.Y., Ko, H.J., Keller, S.R., Kim, J.K., Magnuson, M.A., and Harris, T.E. (2010). Fat cell-specific ablation of rictor in mice impairs insulin-regulated fat cell and whole-body glucose and lipid metabolism. Diabetes *59*, 1397–1406.

Lamming, D.W., Ye, L., Katajisto, P., Goncalves, M.D., Saitoh, M., Stevens, D.M., Davis, J.G., Salmon, A.B., Richardson, A., Ahima, R.S., et al. (2012). Rapamycin-induced insulin resistance is mediated by mTORC2 loss and uncoupled from longevity. Science *335*, 1638–1643.

Laplante, M., and Sabatini, D.M. (2012). mTOR signaling in growth control and disease. Cell *149*, 274–293.

Lee, K.Y., Russell, S.J., Ussar, S., Boucher, J., Vernochet, C., Mori, M.A., Smyth, G., Rourk, M., Cederquist, C., Rosen, E.D., et al. (2013). Lessons on conditional gene targeting in mouse adipose tissue. Diabetes *62*, 864–874.

Martinez-Lopez, N., Athonvarangkul, D., Sahu, S., Coletto, L., Zong, H., Bastie, C.C., Pessin, J.E., Schwartz, G.J., and Singh, R. (2013). Autophagy in Myf5+ progenitors regulates energy and glucose homeostasis through control of brown fat and skeletal muscle development. EMBO Rep. *14*, 795–803.

Masui, K., Tanaka, K., Akhavan, D., Babic, I., Gini, B., Matsutani, T., Iwanami, A., Liu, F., Villa, G.R., Gu, Y., Campos, C., Zhu, S., Yang, H., Yong, W.H., Cloughesy, T.F., Mellinghoff, I.K., Cavenee, W.K., Shaw, R.J., and Mischel, P.S. (2013). mTOR complex 2 controls glycolytic metabolism in glioblastoma through FoxO acetylation and upregulation of c-Myc. Cell Metab. *18*, 726–739.

Mizuarai, S., Miki, S., Araki, H., Takahashi, K., and Kotani, H. (2005). Identification of dicarboxylate carrier Slc25a10 as malate transporter in de novo fatty acid synthesis. J. Biol. Chem. *280*, 32434–32441.

Mullican, S.E., Tomaru, T., Gaddis, C.A., Peed, L.C., Sundaram, A., and Lazar, M.A. (2013). A novel adipose-specific gene deletion model demonstrates potential pitfalls of existing methods. Mol. Endocrinol. *27*, 127–134.

Muzumdar, M.D., Tasic, B., Miyamichi, K., Li, L., and Luo, L. (2007). A global double-fluorescent Cre reporter mouse. Genesis *45*, 593–605.

Nedergaard, J., and Cannon, B. (2010). The changed metabolic world with human brown adipose tissue: therapeutic visions. Cell Metab. *11*, 268–272.

Nedergaard, J., and Cannon, B. (2013). How brown is brown fat? It depends where you look. Nat. Med. *19*, 540–541.

Ohno, H., Shinoda, K., Ohyama, K., Sharp, L.Z., and Kajimura, S. (2013). EHMT1 controls brown adipose cell fate and thermogenesis through the PRDM16 complex. Nature *504*, 163–167.

Pearce, L.R., Komander, D., and Alessi, D.R. (2010). The nuts and bolts of AGC protein kinases. Nat. Rev. Mol. Cell Biol. *11*, 9–22.

Sanchez-Gurmaches, J., and Guertin, D.A. (2014). Adipocytes arise from multiple lineages that are heterogeneously and dynamically distributed. Nat. Commun. *5*, 4099.

Sanchez-Gurmaches, J., Hung, C.M., Sparks, C.A., Tang, Y., Li, H., and Guertin, D.A. (2012). PTEN loss in the Myf5 lineage redistributes body fat and reveals subsets of white adipocytes that arise from Myf5 precursors. Cell Metab. *16*, 348–362.

Sarbassov, D.D., Guertin, D.A., Ali, S.M., and Sabatini, D.M. (2005). Phosphorylation and regulation of Akt/PKB by the rictor-mTOR complex. Science *307*, 1098–1101.

Schulz, T.J., and Tseng, Y.H. (2013). Brown adipose tissue: development, metabolism and beyond. Biochem. J. *453*, 167–178.

Schulz, T.J., Huang, P., Huang, T.L., Xue, R., McDougall, L.E., Townsend, K.L., Cypess, A.M., Mishina, Y., Gussoni, E., and Tseng, Y.H. (2013). Brown-fat paucity due to impaired BMP signalling induces compensatory browning of white fat. Nature *495*, 379–383.

Seale, P., Bjork, B., Yang, W., Kajimura, S., Chin, S., Kuang, S., Scimè, A., Devarakonda, S., Conroe, H.M., Erdjument-Bromage, H., et al. (2008). PRDM16 controls a brown fat/skeletal muscle switch. Nature *454*, 961–967.

Shiota, C., Woo, J.T., Lindner, J., Shelton, K.D., and Magnuson, M.A. (2006). Multiallelic disruption of the rictor gene in mice reveals that mTOR complex 2 is essential for fetal growth and viability. Dev. Cell *11*, 583–589.

Tallquist, M.D., Weismann, K.E., Hellström, M., and Soriano, P. (2000). Early myotome specification regulates PDGFA expression and axial skeleton development. Development *127*, 5059–5070.

Townsend, K.L., and Tseng, Y.H. (2014). Brown fat fuel utilization and thermogenesis. Trends Endocrinol. Metab. *25*, 168–177.

Tseng, Y.H., Butte, A.J., Kokkotou, E., Yechoor, V.K., Taniguchi, C.M., Kriauciunas, K.M., Cypess, A.M., Niinobe, M., Yoshikawa, K., Patti, M.E., and Kahn, C.R. (2005). Prediction of preadipocyte differentiation by gene expression reveals role of insulin receptor substrates and necdin. Nat. Cell Biol. *7*, 601–611.

Tseng, Y.H., Kokkotou, E., Schulz, T.J., Huang, T.L., Winnay, J.N., Taniguchi, C.M., Tran, T.T., Suzuki, R., Espinoza, D.O., Yamamoto, Y., et al. (2008). New role of bone morphogenetic protein 7 in brown adipogenesis and energy expenditure. Nature *454*, 1000–1004.

Tseng, Y.H., Cypess, A.M., and Kahn, C.R. (2010). Cellular bioenergetics as a target for obesity therapy. Nat. Rev. Drug Discov. *9*, 465–482.

Wang, F., Mullican, S.E., DiSpirito, J.R., Peed, L.C., and Lazar, M.A. (2013). Lipoatrophy and severe metabolic disturbance in mice with fat-specific deletion of PPARγ. Proc. Natl. Acad. Sci. USA *110*, 18656–18661.

Yao, Y., Suraokar, M., Darnay, B.G., Hollier, B.G., Shaiken, T.E., Asano, T., Chen, C.H., Chang, B.H., Lu, Y., Mills, G.B., et al. (2013). BSTA promotes mTORC2-mediated phosphorylation of Akt1 to suppress expression of FoxC2 and stimulate adipocyte differentiation. Sci. Signal. *6*, ra2.

Yuan, M., Pino, E., Wu, L., Kacergis, M., and Soukas, A.A. (2012). Identification of Akt-independent regulation of hepatic lipogenesis by mammalian target of rapamycin (mTOR) complex 2. J. Biol. Chem. *287*, 29579–29588.